Mechanical and tomographic characterisation of recycled Carbon Fibre Reinforced Polymer (rCFRP) using a fully mechanical environmentally friendly process

Andrea Casaroli, Marco V. Boniardi, Edoardo Scabini
Department of Mechanical Engineering, Politecnico di Milano, via La Masa 1, 20156 Milano, Italy
andrea.casaroli@polimi.it, https://orcid.org/0000-0001-5207-5547
marco.boniardi@polimi.it, https://orcid.org/0000-0002-2438-7890
edoardo.scabini@polimi.it, https://orcid.org/0009-0005-4487-912X

ABSTRACT. The widespread use of carbon fibre-reinforced polymer (CFRP) composites in sectors such as aerospace and aviation calls for the adoption of sustainable recycling protocols. This research evaluates the mechanical and tomographic characterisation of recycled CFRP obtained via an innovative fully mechanical sustainable process. Thin (0.8 mm) and thick (2.0 mm) recycled non-woven fabric fibre laminates were subjected to uniaxial tensile testing in accordance with ASTM D3039M. The results revealed that the thick laminates achieved an UTS of 310-330 MPa and a Young's modulus of 21.3–21.7 GPa in longitudinal direction, whilst the transverse properties were significantly lower. Despite the excellent cleanliness of the fibres, the mechanical performance of the composite laminates remains limited. Fractographic analysis using scanning electron microscopy (SEM) and internal volumetric evaluation using X-ray micro-tomography revealed severe spatial inhomogeneity in the distribution of the recycled fibres. Dense fibre bundles impeded the microscopic capillary infiltration of the resin, generating critical volumetric porosity and jagged shrinkage voids that act as severe stress concentrators. Consequently, it is essential to optimise the spatial uniformity within the mat of recycled precursors in order to reduce internal defects and fully exploit the structural potential of mechanically recycled CFRP.

KEYWORDS. Recycled Carbon Fibre Reinforced Polymers (rCFRP), Mechanical Characterization, X-ray Micro-tomography, Fractography, Impregnation Dynamics, Volumetric Porosity.

Citation: Casaroli, A., Boniardi, M. V., Scabini, E., Mechanical and tomographic characterisation of recycled Carbon Fibre Reinforced Polymer (rCFRP) using a fully mechanical environmentally friendly process, Fracture and Structural Integrity, 77 (2026) 89-106.

Received: 23.03.2026
Accepted: 13.04.2026
Published: 16.04.2026
Issue: 07.2026

INTRODUCTION

Over the past decade, the global materials market has witnessed a radical transformation toward the integration of advanced carbon composite systems. This evolution is primarily based on the exceptional mechanical properties offered by these materials, which have found their greatest application in the aerospace and aeronautical sectors. In these sectors, the convergence of high tensile strength, structural stiffness, and low specific weight represents a fundamental engineering goal. Reducing airframe weight is directly proportional to reducing fuel consumption, one of the largest operating costs in the aeronautical sector, while also enabling increased payload capacity and reduced polluting emissions.

Unlike traditional isotropic metal alloys [1] [2] [3], carbon composites can exhibit either quasi-isotropic behaviour or marked anisotropy, depending on length, direction and orientation of the reinforcing fibres.

This characteristic gives engineers the unique ability to tailor a system's structural response to specific external loads, enabling precise control of critical frequencies and vibrational responses. This utility is exemplified by helicopter rotor blades, where carbon fibre composites have replaced traditional materials that were previously too brittle to withstand the high-frequency cyclic stresses inherent in rotor dynamics [4][5].

Furthermore, the industrial success of CFRPs is attributed to the versatility of their manufacturing processes. These techniques enable the fabrication of complex geometries with a level of simplicity and weight efficiency that cannot be matched by conventional metal forming or machining [6] [7]. By using continuous fibre architectures, designers can eliminate numerous mechanical joints, thus reducing the overall number of components and minimizing weight and potential failure points associated with fasteners.

A composite material is defined as a heterogeneous system formed by the union of two or more physically distinguishable phases, resulting in mechanical properties superior to those of the individual constituents. Within the composite hierarchy, which includes metal matrix composites (MMCs) and ceramic matrix composites (CMCs), CFRPs are classified as polymer matrix composites (PMCs). These systems are essentially composed of three regions: (i) the reinforcing phase, (ii) the polymer matrix, and (iii) the interface.

In typical high-performance CFRP applications, the reinforcing fibres occupy between 50% and 70% of the total volume [8] [9]. While the fibres serve as the primary load-bearing component, the matrix ensures load distribution among the fibres and provides resistance to compressive and shear forces.

The mechanical profile of the final composite is highly dependent on the choice of carbon fibre precursor. Industrial carbon fibre production generally follows two distinct routes: polyacrylonitrile (PAN) and pitch [10]. The PAN-based process, which accounts for approximately 90% of global production, involves the polymerization, oxidation, and carbonization of acrylonitrile molecules. The resulting fibres are characterized by graphitic layers that, while aligned along the fibre axis, exhibit a crystalline disorientation that confers high tensile strength but relatively low ductility.

In contrast, pitch fibres are derived from the polymerization of petroleum residues or tar. As summarized in Tab. 1 [10], these precursors produce significantly different mechanical properties.

	PAN fibres	Pitch fibres
UTS (Ultimate Tensile Strength) [MPa]	3500 - 6300	1300 - 3100
E (Young's modulus) [GPa]	200 - 500	150 - 900
A% (Elongation after fracture) [%]	0.8 - 2.2	0.3 – 0.9
ϱ (Density) [g/cm^3]	1.7 - 1.8	1.8 - 2.2

Table 1: Mechanical properties interval typical for PAN and Pitch fibres [10].

Based on their elastic modulus (E), carbon fibres are commercially categorized into Standard Modulus (SM: E < 250 GPa), Intermediate Modulus (IM: E < 320 GPa), High Modulus (HM: E < 440 GPa), and Ultra High Modulus (UHM: E > 440 GPa). Each fibre typically possesses a diameter ranging from 5 μm to 10 μm and is bundled into wires containing approximately 10^3 to 10^5 filaments [11].

The arrangement of fibres within the matrix is a primary determinant of the composite's macroscopic behaviour. Fig. 1 provides a classification of these dispositions, ranging from short-fibre mats to continuous fibre weaves. Short fibres, such as those found in Sheet Moulding Compounds (SMC) and Bulk Moulding Compounds (BMC), are often incorporated

into vinyl ester matrices via compression moulding. Due to the random orientation of the fibres, these materials exhibit a quasi-isotropic behaviour.

In contrast, long-fibre reinforcements are utilized where high static mechanical performance is required. These include unidirectional fibres, which offer the highest strength along a single axis, and weaved fabrics [12]. Weaved fibres have become the preferred choice for modern applications due to their superior damage tolerance, fatigue resistance, and ease of manufacturing through the use of pre-impregnated (prepreg) materials.

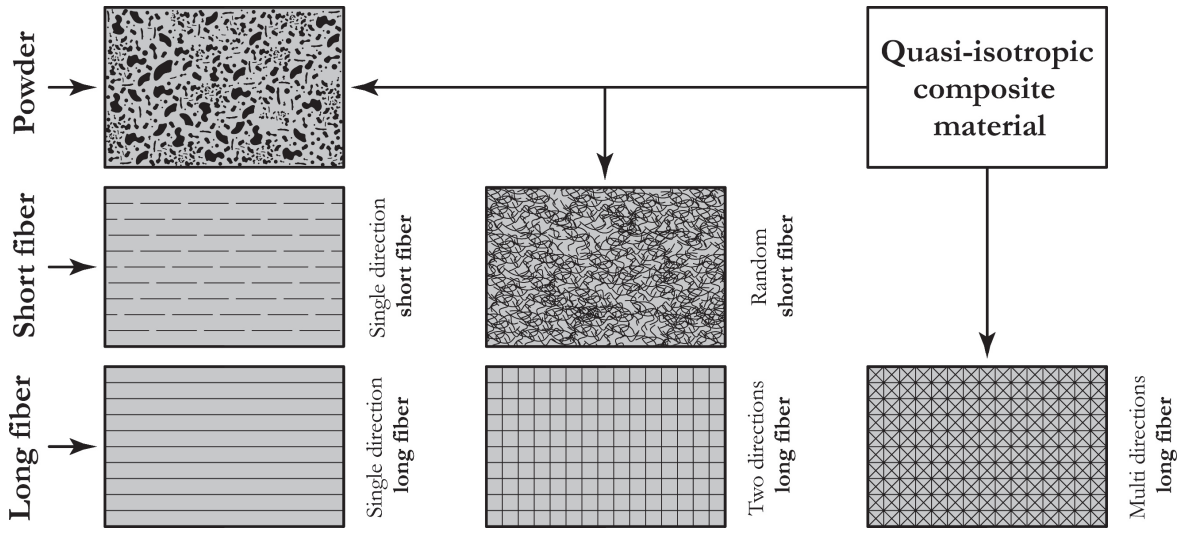

Figure 1: Schematic classification of the arrangements of reinforcing fibres.

As shown in Fig. 2, several standard weaving patterns exist, each offering a specific balance between stability and conformability.

- *Plain Weave:* highly stable but the least flexible, making it difficult to adapt to complex, highly curved surfaces.
- *Twill Weave:* a popular compromise between stability and flexibility, frequently used in the automotive sector for its aesthetic symmetry and balanced isotropy.
- *Satin Weave* (*e.g., Eight Harness Satin*): characterized by high flexibility and drape-ability, allowing it to conform to intricate geometries, though at the cost of reduced stability and increased anisotropy.

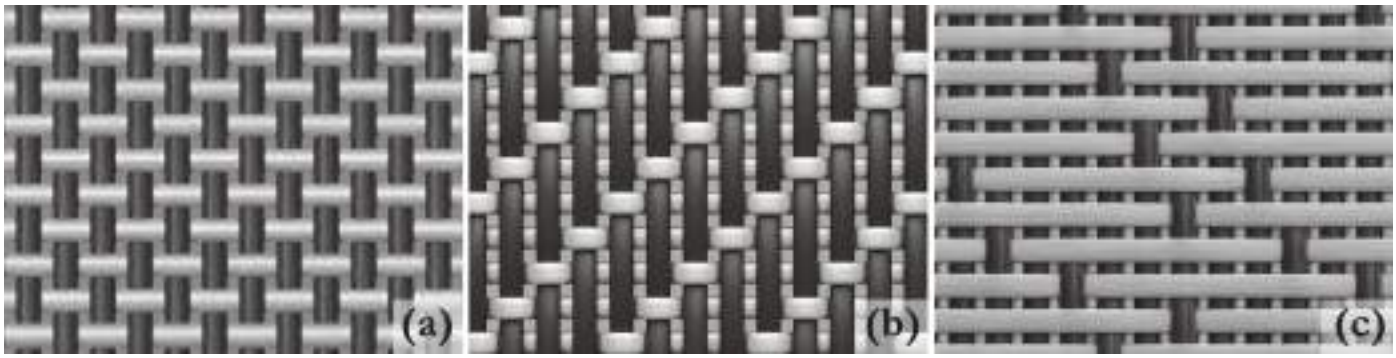

Figure 2: Standard weaving patterns used by composite industries: (a) Plain, (b) Twill and (c) Eight Harness Satin Weave.

The polymer matrix is essential for protecting the fibres from environmental degradation and ensuring the integrity of the structural system. Polymers are broadly divided into thermoplastic and thermoset categories. Thermoset polymers, specifically high-performance epoxy resins, are the standard for aerospace applications due to their superior adhesion, chemical resistance, and stiffness [13]. The properties of a typical aerospace-grade epoxy resin are detailed in Tab. 2 [14].

One of the main engineering constraints of polymer matrices is the glass transition temperature (T_g). Above this temperature, the crystalline or semi-ordered structure of the polymer disperses, resulting in a significant loss of mechanical properties. Furthermore, the difference in thermal expansion coefficients between the matrix (high) and the carbon fibres (low, approximately 0.1 x 10^{-6} K^{-1} [9]) can induce internal stresses that compromise interfacial bonding.

UTS (Ultimate Tensile Strength) [MPa]	55 - 130
E (Young's modulus) [GPa]	2.75 - 4.10
ν (Poisson coefficient)	0.20 - 0.33
ϱ (Density) [g/cm^3]	1.2 - 1.3
λ (Thermal expansion coefficient) [K^{-1}]	$50 \cdot 10^{-6}$ - $80 \cdot 10^{-6}$

Table 2: Mechanical properties interval typical for high-performance epoxy resins for aerospace applications [14].

The interface is the critical region where stress is transferred from the matrix to the reinforcing fibres. The efficiency of this transfer is determined by the "wettability" of the fibres, characterized by the contact angle between the liquid polymer and the solid surface of the fibre. Bonding mechanisms at the interface are classified as:
- *Mechanical Bonding:* driven by fibre surface roughness and friction.
- *Physical Bonding:* resulting from low-intensity Van der Waals forces.
- *Chemical Bonding:* the strongest form of adhesion, including reaction bonding.

Reaction bonding is a diffusion-controlled process, and its kinetics are described by the diffusivity (1) that shows interfacial bond quality is exponentially dependent on the thermal parameters of the manufacturing process.

$$D = D_0 \cdot e^{-\frac{E_A}{R \cdot T}} \tag{1}$$

where:
- D is the diffusivity (or diffusion coefficient) [m^2/s],
- D_0 is the maximal diffusion coefficient [m^2/s],
- E_A is the activation energy for diffusion [J/mol],
- R is the universal gas constant [8.31446 J/(mol·K)],
- T is the absolute temperature [K].

Despite the undeniable performance advantages of CFRPs, their environmental and economic sustainability remain significant challenges. The three-dimensional covalent network of thermoset resins means they cannot be melted and reshaped. As global consumption of carbon fibre-reinforced plastics (CFRPs) continues to increase in the aerospace, aviation, automotive, and energy sectors, managing end-of-life (EOL) products and production waste has emerged as a key challenge for materials engineering.

The high level of technology required to produce carbon fibres, which are primarily derived from polyacrylonitrile (PAN) or pitch-based precursors, means the material retains considerable residual value even at the end of its primary life cycle. Consequently, failure to implement effective recovery strategies results not only in an environmental burden but also in a substantial loss of the intrinsic economic and structural value of the waste material.

Current research initiatives and industry consortia are focused on bridging the gap between the performance of virgin fibre and the utility of recycled fibre [15]. The primary goal is to develop recovery processes that produce recycled carbon fibres capable of directly competing with virgin alternatives in secondary high-performance applications. However, the feasibility of fibre recovery is inherently limited by the complex architecture of the composite itself; specifically, by the difficulty of extracting high-modulus fibres from a cross-linked thermoset or thermoplastic polymer matrix without inducing significant mechanical or chemical degradation.

Currently proposed strategies for extracting carbon fibres from the matrix can be systematically classified into three main functional domains: thermal, chemical, and mechanical recycling. Each of these pathways presents a unique set of advantages and disadvantages in terms of maintaining fibre length, surface integrity and energy intensity.

Mechanical recycling, which typically involves grinding or milling processes, represents a mature technology with a high Technology Readiness Level (TRL). In this approach, the composite is physically broken down into smaller fragments, resulting in a mixture of resin and shortened fibres.

For carbon fibres, however, mechanical grinding is often considered a "downcycling" process, as it significantly reduces the fibres' aspect ratio, limiting their use to fillers or reinforcements in low-stress injection-moulded components rather than structural laminates. Thermal recycling, specifically pyrolysis, is one of the most developed high-tech solutions for carbon fibre recovery [16]. This process involves the thermal decomposition of the polymer matrix in an inert atmosphere,

effectively "burning" the resin to release the carbon fibres. Thermal processes can lead to a steady degradation of mechanical properties, making the recycled material significantly weaker than its virgin counterpart. For carbon fibres, the economic viability of thermal plants depends heavily on processing large volumes of material. The energy required to reach the decomposition temperatures of high-performance resins must be balanced with the market price of the recovered fibres.
If degradation is too severe, potential customers may opt for new virgin fibres, thus limiting the market for recycled products.
Chemical recycling uses solvents and catalysts to break the chemical bonds of the polymer matrix at relatively lower temperatures than pyrolysis [17]. This method is highly effective for fibre recovery with minimal surface damage and greater length retention. However, like thermal methods, chemical recycling requires sophisticated industrial infrastructure and is currently subject to rigorous evaluation regarding its economic feasibility and chemical waste stream management [18]. The choice of a recycling route is governed by a balance between the technology readiness level (TRL) and the waste treatment hierarchy (WTH). Traditional disposal methods, such as landfill, have the highest TRL score, indicating a fully mature and accessible "technology." However, landfill has the lowest possible WTH score, indicating its complete failure as a sustainable solution. From an economic perspective, the costs associated with landfill disposal are borne directly by the consumer, while the entire technological value of the composite is lost forever. This creates a strong incentive to switch to high-tech recovery. The challenge is that recycled fibres are not intrinsically equivalent to virgin fibres; specific differences in surface chemistry and mechanical strength influence the consumer's choice between virgin and recycled raw materials. In the short term, the carbon fibre recycling market is driven by the relatively low cost of recovery compared to the energy-intensive processes required to produce virgin PAN. For carbon fibres to achieve a truly circular lifecycle, the industry must overcome the economic barriers associated with high-tech processing facilities. Only by ensuring that recycled fibres can compete, both in terms of performance and cost, with virgin materials can the technological value associated with these advanced materials be preserved for future generations of engineering applications. As the market value of carbon fibres is expected to approach that of glass fibres in the next 15–20 years [19], the development of industrial-scale recycling solutions is no longer a marginal issue but a necessity for a sustainable composites market. This article aims to provide a comprehensive analysis of the mechanical and tomographic characterization of recycled CFRP obtained through an innovative, entirely mechanical, and environmentally sustainable process [20].

RESULTS AND DISCUSSION

Materials and method

A detailed analysis was carried out to assess the mechanical behaviour of recycled CFRP produced using an innovative fully mechanical and environmentally sustainable process [20]. The main objective of this comprehensive series of analyses - which included Scanning Electron Microscopy of recycled non-woven fabric mats and carbon fibre powders, tensile tests on epoxy-impregnated carbon panels, and high-resolution tomographic analysis - was to systematically identify any latent issues within the recycling process. Ultimately, understanding these phenomena aims to formulate specific guidelines capable of improving the production quality and reliability of recycled carbon composite panels made of recycled CFRP. The samples provided for mechanical and tomographic evaluation consisted of two different types of recycled carbon panels, both produced by the controlled impregnation of recycled carbon fibre non-woven fabric mats with a standard structural epoxy resin.

SEM analysis of recycled fibre non-woven fabric mats

This analysis aims to characterise the morphology and degree of cleanliness of the fibres through a Scanning Electron Microscope (SEM) analysis. The advantages offered by this instrument are considerable and clearly explain why it is used: high resolution, high magnification and a wide depth of field. These characteristics allow for an accurate visualisation of the fibres present in the non-woven fabric samples; thanks to the depth of field, it is possible to analyse the surfaces of the fibres at different distances from the focal point. The material supplied consists of two non-impregnated recycled carbon non-woven fabric mats, with a weight per unit area of 200 g/m² and 1000 g/m².
The analysed areas, approximately 9 cm² in size, were randomly selected from the non-woven fabric mats. Fig. 3 shows the areas observed at 150x, 2000x, and 4000x magnifications. Although the fibres appear to be distributed almost randomly, a certain amount of them, estimated between 5% and 20% depending on the observation area, group together in bundles with preferential orientations. Furthermore, the same fibre density is observed regardless of the weight per unit area considered. Higher magnifications allow to observe the excellent level of cleanliness of the recycled fibres, achieved thanks to the innovative, entirely mechanical recycling process [20]. Only small amounts of residual material, likely deriving from

the previous polymer matrix, are present on the fibres. The recycled fibres show no visible deterioration. The average fibre diameter, verified by SEM analysis, is approximately between 7.0-7.5 μm.

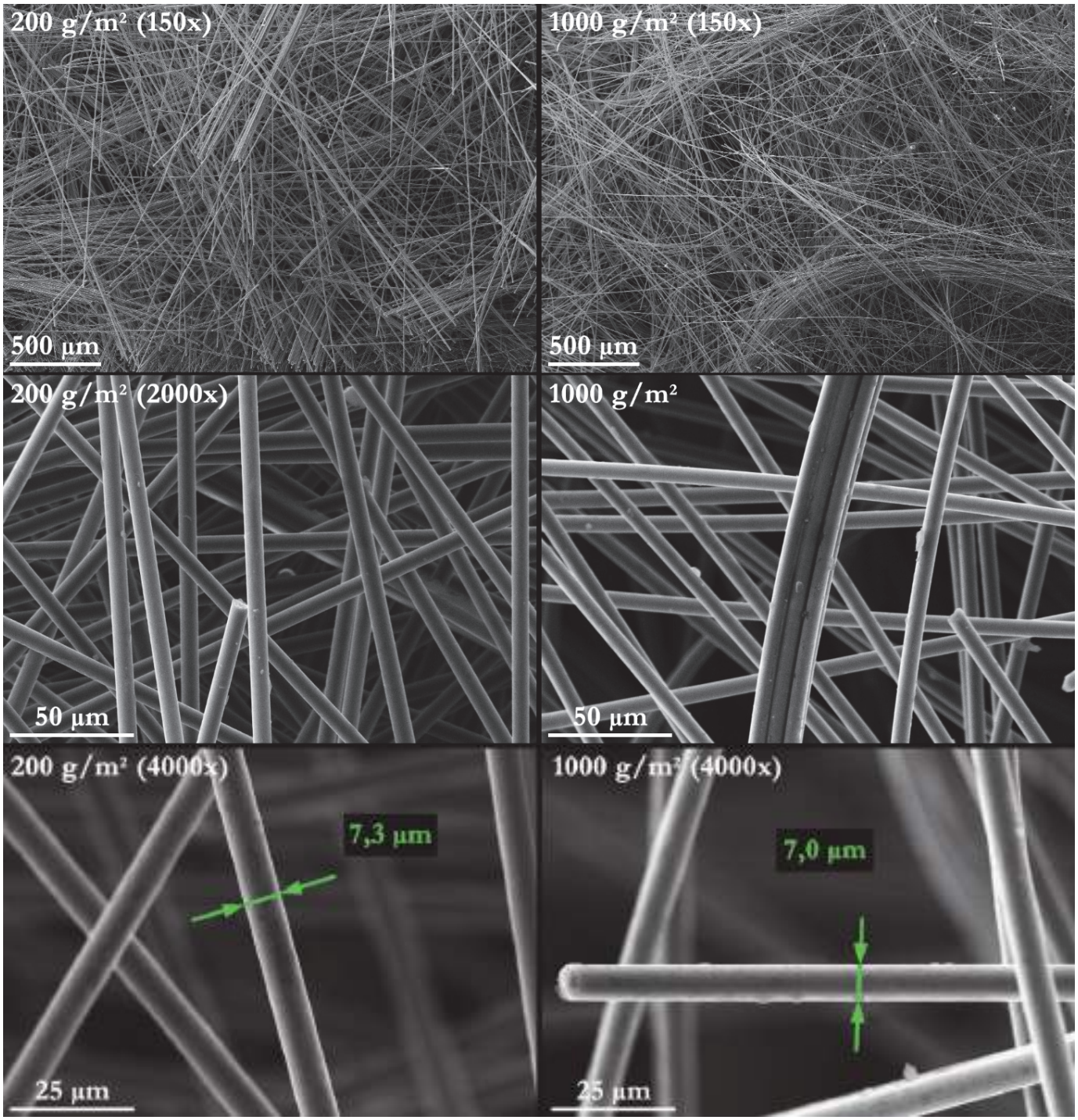

Figure 3: SEM analysis with secondary electrons of two non-impregnated recycled carbon non-woven fabric mats, with weight per unit area of (left) 200 g/m² and (right) 1000 g/m² (magnifications: 150x, 2000x and 4000x).

SEM analysis of recycled fibre powder

SEM analysis is aimed to characterize the shape and cleaning level of the fibre powder considered as a by-product of the innovative recycling process [20]. The powder sample has a declared nominal length of 10 μm. Fig. 4 shows secondary and backscattered electron analysis at 500x, 1000x, and 5000x magnifications. Secondary electron analysis shows that the fibre length has values between 20 μm and 80 μm, exceeding the declared 10 μm. Furthermore, the presence of residues on the

surface of the fibres can be observed, which are traces of resin from the previous polymer matrix. Backscattered electron and X-ray microchemical analysis reveal the presence of less than 1% particles composed of Al, Si, and Ca, which likely originate from glass fibres or ceramic particles from the grinding system used in the recycling process.

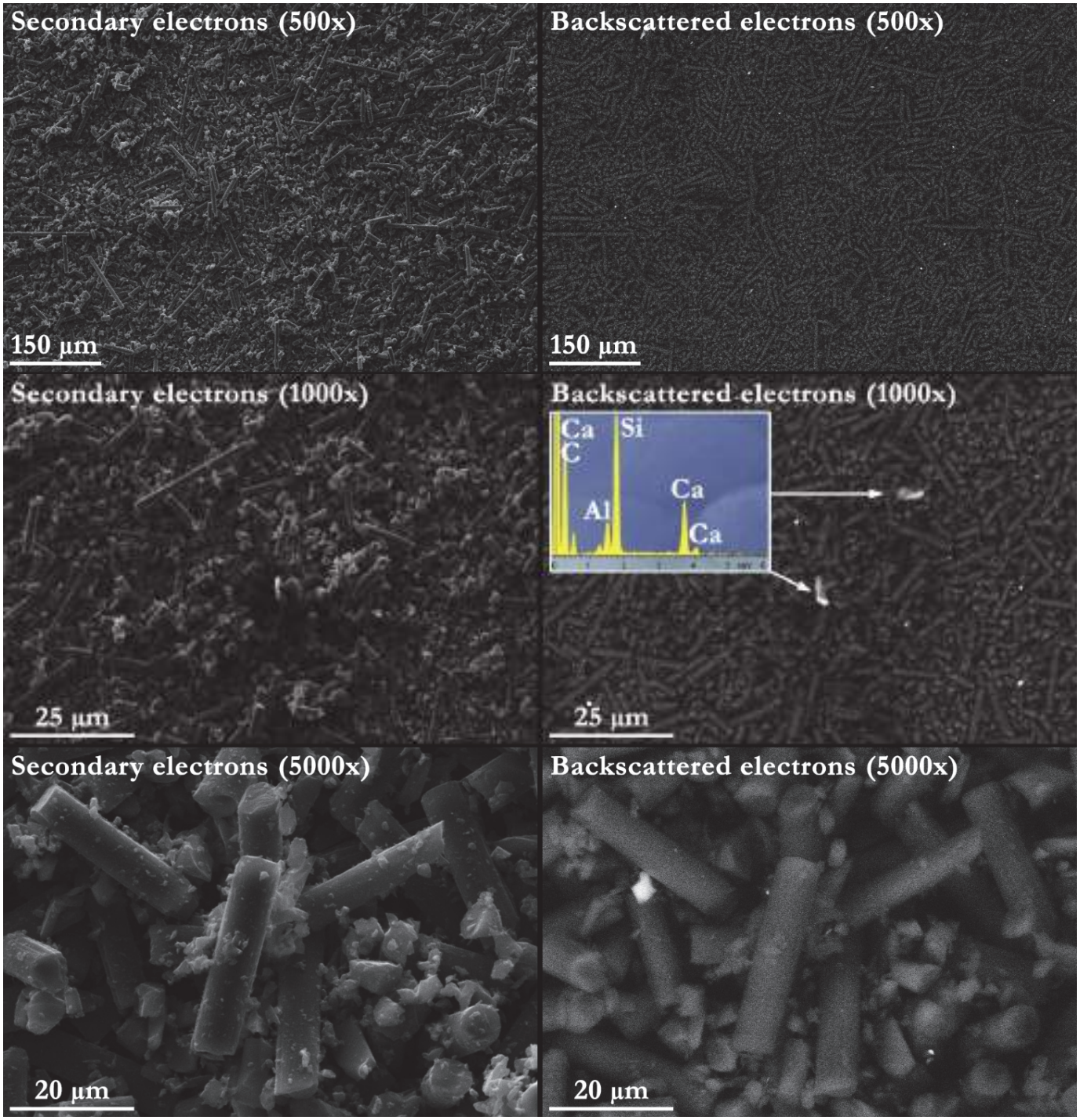

Figure 4: SEM analysis of recycled fibre powder with secondary (left) and backscattered (right) electrons at 500x, 1000x, and 5000x magnifications.

Tensile tests

To facilitate a comparative analysis of the effects of thickness and the volumetric distribution of defects on tensile properties, the material were divided into two different laminate configurations:

1. *Thin laminate:* this configuration possessed a nominal thickness of 0.8 mm and was fabricated from a single ply of recycled carbon fibre non-woven fabric mat with a weight per unit area of 300 g/m². The macroscopic dimensions of the resulting rectangular panel were 280x240 mm. Gravimetric analysis of the constituent phases revealed a composition of 21 g of recycled carbon fibre and 55 g of the epoxy resin, indicating a highly resin-rich macroscopic architecture.
2. *Thick laminate:* this structural configuration exhibited a nominal thickness of 2.0 mm and was manufactured by sequentially overlaying two distinct recycled carbon fibre non-woven fabric mats, each possessing a weight per unit area of 300 g/m². The spatial dimensions of the panel were identical to the thin variant, measuring 280x240 mm. The gravimetric composition consisted of 46 g of recycled carbon fibre matrixed within 117 g of epoxy resin.

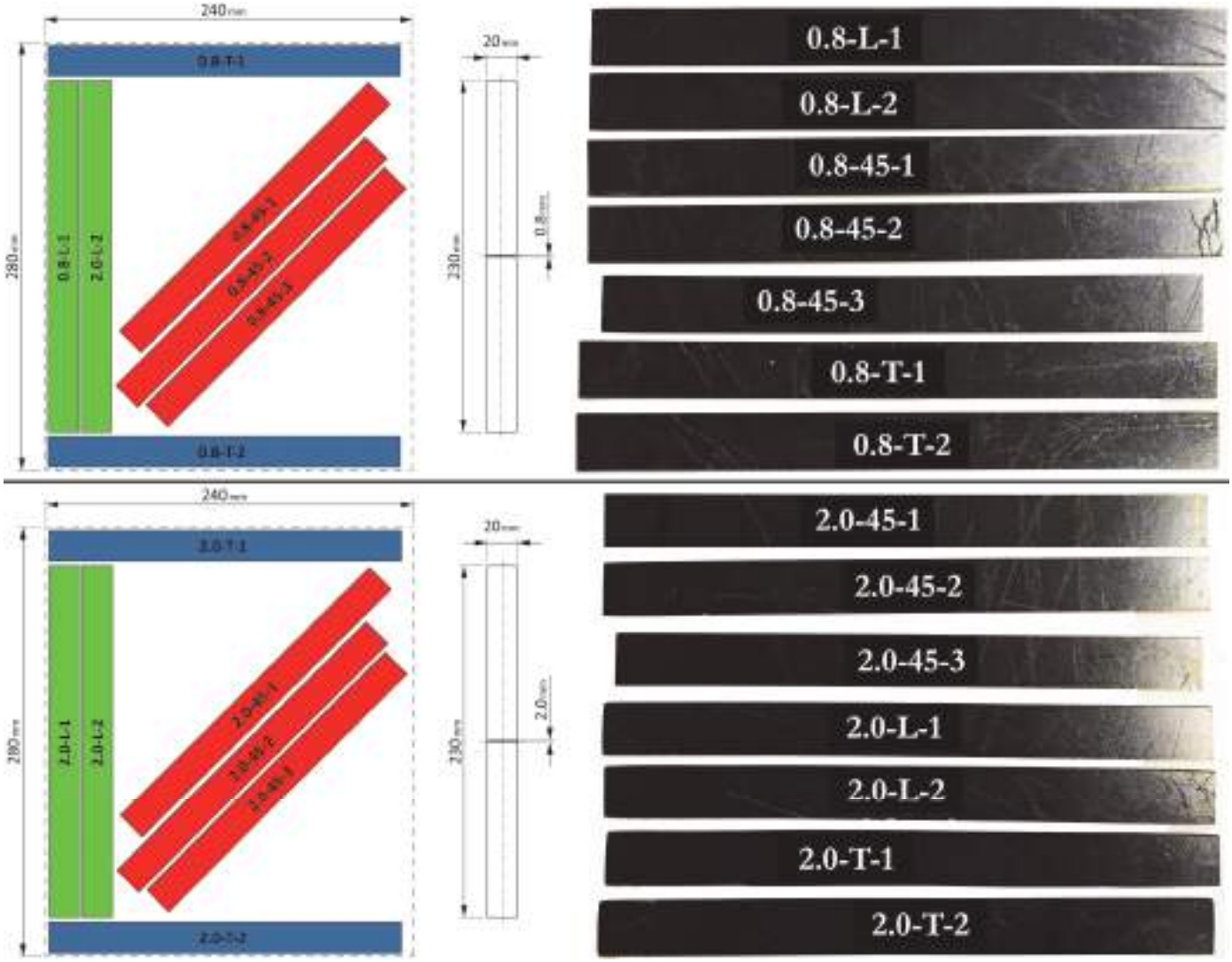

Figure 5: Tensile test specimens (right) and their shapes and positions (left) on thin and thick laminates.

To rigorously quantify the tensile properties of recycled carbon panels, a series of uniaxial tensile tests were performed. The experimental procedure was conducted in strict accordance with internationally recognized standardization protocols, detailed in ASTM D3039M, *"Standard Test Method for Tensile Properties of Polymer Matrix Composites"*. Specimens were cut from the original panels using precision waterjet cutting; furthermore, to mitigate the influence of premature crack initiation from edge defects, the cut surfaces of each specimen were meticulously polished to reduce the arithmetic mean roughness (R_a) to below 1.6 μm. In strict accordance with the geometric recommendations outlined in ASTM D3039M, the nominal dimensions of the specimens were standardized to 230 x 20 mm. A critical aspect of composite characterization is the assessment of the material's directional influence.

Consequently, the potential anisotropy of the recycled panels was systematically verified by varying the direction of the samples with respect to the main axis of the fibre mat. The tests were conducted along three main orientations: the longitudinal direction, 45° angle, and the transverse direction (Fig. 5).
The tensile test results, summarized in Tab. 3 and Fig. 6, show significant trends in the behaviour of the recycled composites for both laminate thicknesses.

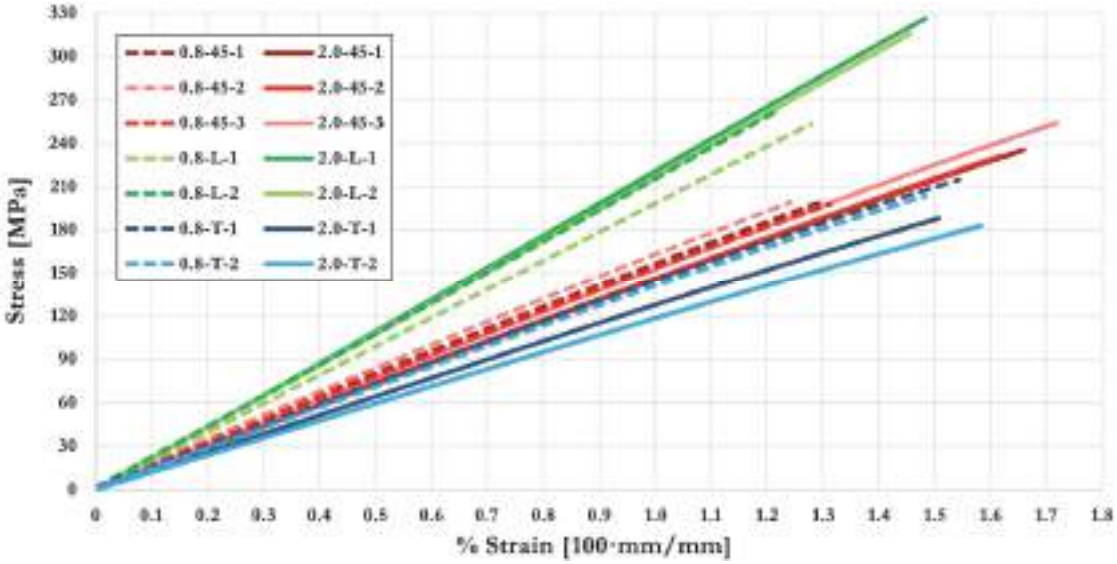

Figure 6: Stress-strain curves of thin (dashed lines) and thick (solid lines) laminates along the longitudinal (green), 45° angle (red) and transverse (blue) directions.

	Thin laminate			Thick laminate		
	Longitudinal	45°	Transverse	Longitudinal	45°	Transverse
UTS [MPa] (Ultimate Tensile Strength)	250-260	200	200-220	310-330	230-260	180-190
A% [%] (Elongation after fracture)	1.20-1.30	1.25-1.30	1.45-1.55	1.40-1.50	1.60-1.70	1.50-1.60
E [GPa] (Young's modulus)	19.5-21.0	15.3-16.5	14.1-14.4	21.3-21.7	14.5-15.3	11.8-12.8

Table 3: Mechanical properties of thin and thick laminates along the longitudinal, 45° angle and transverse directions.

For the thin laminate (0.8 mm), the longitudinal orientation showed an Ultimate Tensile Strength (UTS) between 250 MPa and 260 MPa, an elongation after fracture (A%) of 1.20%-1.30%, and a Young's modulus (E) between 19.5 GPa and 21.0 GPa. When tested at 45° angle, the mechanical properties deteriorated, producing a UTS of 200 MPa, an A% of 1.25%-1.30%, and a substantially lower E, between 15.3 GPa and 16.5 GPa. In the transverse direction, the UTS ranged from 200 MPa to 220 MPa, with an A% ranging from 1.45 to 1.55% and an E ranging from 14.1 GPa to 14.4 GPa.
In contrast, the thicker laminate (2.0 mm) demonstrated higher mechanical strength. In the longitudinal direction, the UTS increased from 310 to 330 MPa, accompanied by an A% ranging from 1.40 to 1.50% and an E ranging from 21.3 GPa to 21.7 GPa. Specimens angled at 45° maintained a relatively high UTS of 230-260 MPa, a higher A% ranging from 1.60% to 1.70% and E ranging from 14.5 GPa to 15.3 GPa. Finally, transverse specimens showed the lowest tensile strength, with a UTS of 180-190 MPa, a A% ranging from 1.50% to 1.60%, and an E ranging from 11.8 GPa to 12.8 GPa.
A critical analysis of the experimental results allows us to draw several conclusions regarding the mechanical behaviour:

- *High anisotropy:* the material behaviour is not absolutely isotropic; both the ultimate tensile strength (UTS) and Young's modulus (E) consistently recorded significantly higher values along the longitudinal direction compared to the 45° angled and transverse orientations.
- *Brittle fracture:* the stress-strain curves revealed a complete absence of any plastic deformation that underscores the classic brittle fracture behaviour of high-stiffness composite materials.
- *Good statistical reliability:* the results showed a high degree of repeatability between the tested samples, serving as a reliable index of good experimental precision.

- *Volumetric Defect Sensitivity:* a direct comparison between the two geometries revealed that the UTS for the thin laminate was consistently lower than the UTS for the thick one. The statistical influence of critical internal defects is functionally lower over a larger cross-sectional area, meaning that UTS increases as the cross-sectional area grows.

Despite the internal consistency of the testing, a comparative analysis against established literature benchmarks revealed a severe performance deficit. Typical rCFRP panels documented in literature, having a fibre volume fraction of approximately 28% (which is similar to the specific gravimetric ratios of the tested specimens), achieve an UTS of 400 - 450 MPa and an E of 30.0 GPa [9]. Literatures also state that rCFRP, using fibres obtained through recycling methodologies which maintain the integrity of the fibre itself and impregnated using optimized processes, can achieve mechanical properties slightly lower or comparable with the ones obtained using virgin fibres with the same length [18][21]. The difference between the theoretical potential and the analysed specimens suggests the presence of severe internal manufacturing defects which limit the mechanical properties of the material. To clarify the specific nature of these performance-limiting defects, a fractographic and tomographic analysis was subsequently conducted.

Tensile tests: SEM analysis of the fracture surfaces

The primary objective of the fractographic analysis was to systematically identify topological evidence of fracture surfaces, thereby obtaining information on the specific failure mechanisms that reduced the tensile strength measured during the tensile tests. An initial visual inspection of the fractured specimens classified the failure morphologies in close accordance with the fracture modes specified in ASTM D3039M. This macroscopic evaluation revealed that the specimen fractures could be classified exclusively as "lateral" or "angled" fractures. It is important to note that this preliminary visual analysis revealed no significant differences in fracture modes between the thin and thick laminates (Fig. 7).

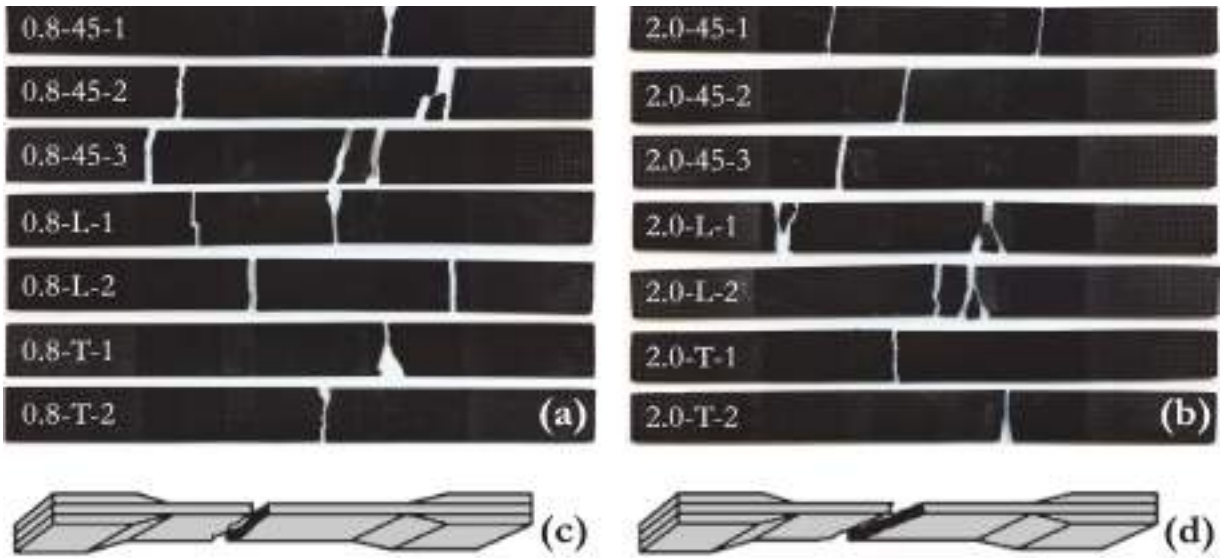

Figure 7: Broken specimens with nominal thickness of 0.8 mm (a) and 2.0 mm (b). (c) and (d) show respectively "lateral" and "angled" fractures modes specified in ASTM D3039M.

Accordingly, high-resolution scanning electron microscopy (SEM) was employed to analyse fracture surfaces. The fundamental assumption was based on the fluid dynamics of the resin impregnation step. The complete infiltration of a fibre mat by a liquid thermosetting resin is determined by the complex interplay of two distinct macroscopic and microscopic fluid flow. The macroscopic flow determines the propagation of the resin through the open interstitial spaces between the individual fibres and is driven primarily by the magnitude of the externally applied injection pressure. In contrast, the microscopic flow governs the localized infiltration of the resin directly into the dense regions within the fibres. The kinetics of this microscopic flow is governed by a more complex set of variables, including external pressure, the contact angle (wettability) between the liquid polymer and the solid fibre, localized capillary pressure and the surface tension [22]. The main factor determining void formation and resulting poor structural impregnation is the velocity difference between these two simultaneous flows. If the microscopic capillary flow advances at a faster rate than the macroscopic flow, air becomes trapped within the macroscopic interstitial channels, leading to the formation of large macro-voids due to the physical impossibility of evacuating the trapped gas.

In the opposite situation, where the macroscopic flow exceeds the microscopic capillary infiltration, the mould cavity fills completely before the individual fibre bundles are fully saturated, directly causing poor diffuse fibre impregnation. SEM analysis of the fracture surfaces (Figs. 8 and 9) provided clear visual confirmation of these phenomena. The analysis revealed the widespread presence of dense fibre bundles with uniform diameters, ranging from 50 μm to 100 μm. These bundles are the result of a highly inhomogeneous spatial distribution of individual carbon fibres within the original recycled fibre mat. During the mechanical moulding process, the applied consolidation pressure compacts these dense, inhomogeneous regions, further increasing fibre agglomeration.

Within these highly concentrated regions, the extreme spatial density of the filaments physically impedes adequate penetration of the viscous epoxy resin. Instead of achieving a uniform infiltration front, the resin is forced to bypass these dense bundles, creating preferential flow paths. This localized disruption of the macroscopic flow front actively prevents homogeneous resin propagation and aggressively promotes large-scale porosity formation.

Furthermore, this non-homogeneous distribution of reinforcing fibres also explains the presence of large, resin-rich areas scattered across the fracture surface. Upon fractographic examination, these localized regions are easily identifiable by the complete absence of reinforcing fibres and the presence of topological features indicative of an extremely brittle fracture, a failure morphology typical of unreinforced, high-strength polymer materials.

The presence of dry, unimpregnated fibre bundles and excessively resin-rich matrices creates a highly dispersed mechanical environment, characterized by high stress concentrations and radically unpredictable load transfer mechanisms, ultimately leading to premature and catastrophic failure.

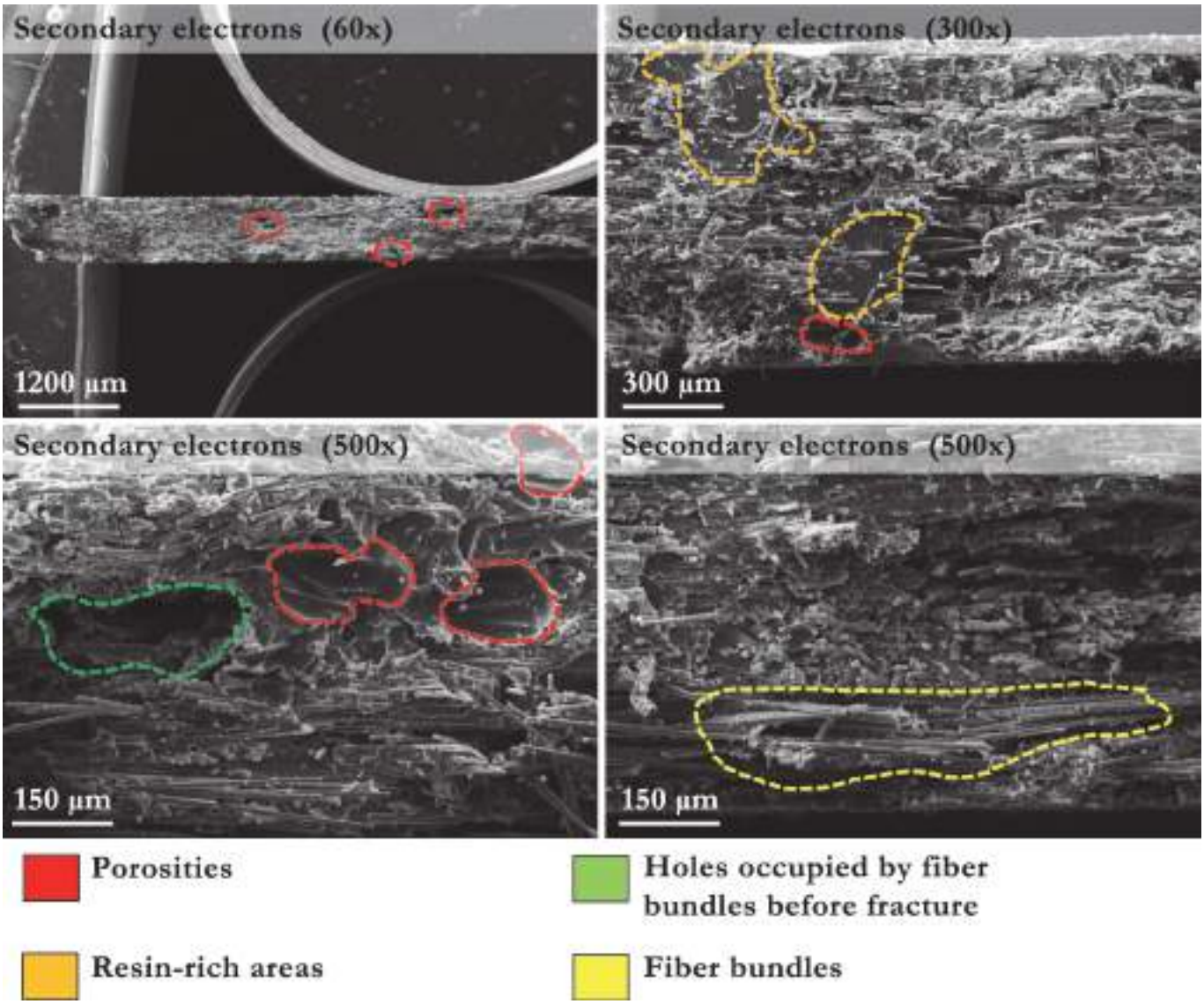

Figure 8: Fracture surface of 0.8-45-1 tensile specimen (0.8 mm thick, 45° angle, first specimen) at increasing magnifications.

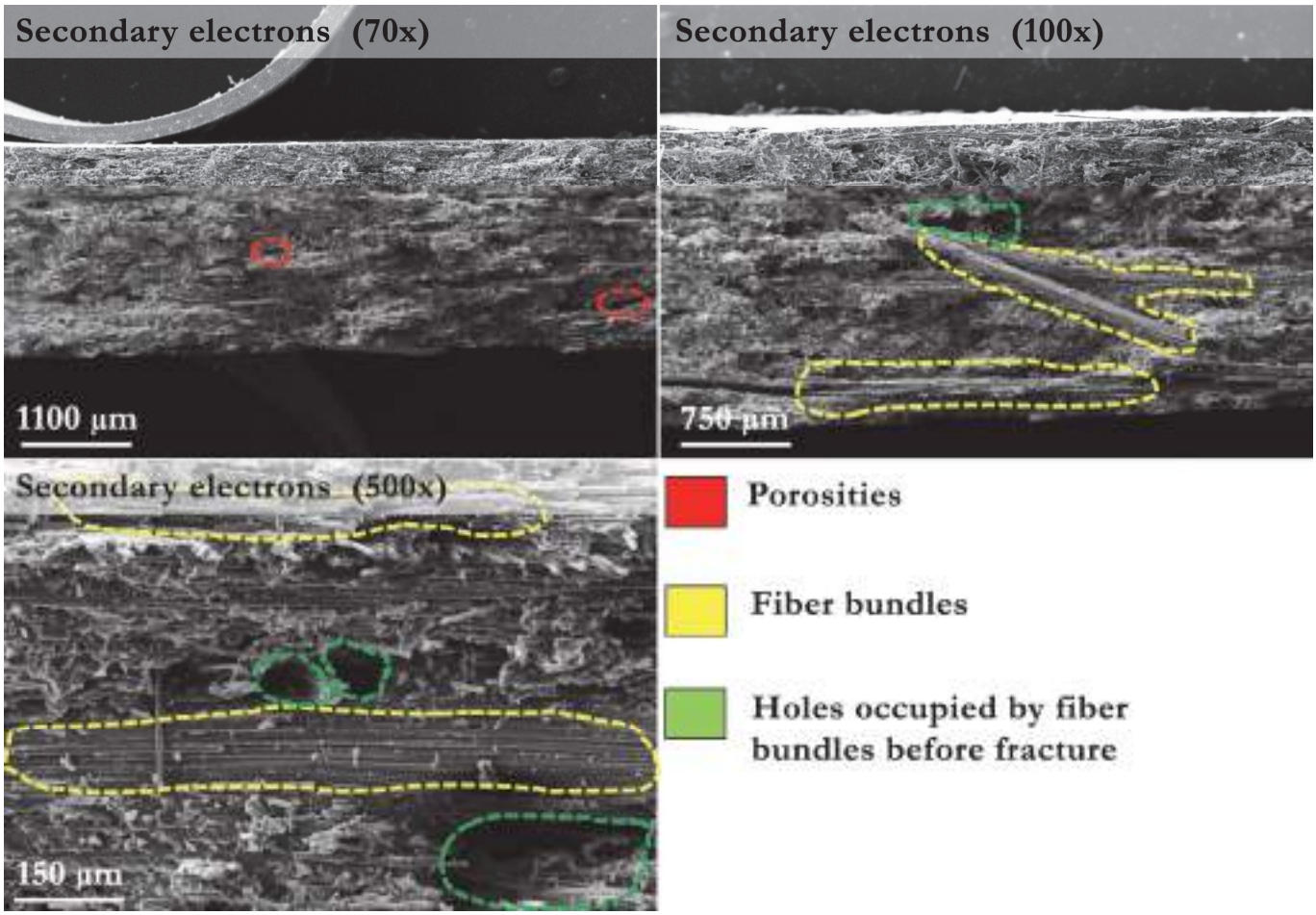

Figure 9: Fracture surface of 2.0-45-1 tensile specimen (2.0 mm thick, 45° angle, first specimen) at increasing magnifications.

Micro-Tomographic investigation: internal defect characterization

To overcome the inherent limitations of two-dimensional surface fractography and obtain a volumetric quantification of the material's internal defects, high-resolution micro-tomographic analysis was performed. The analytical procedure utilized the North Star ImagiX tomograph. Thanks to the differential attenuation of X-rays across phases of different densities, this device facilitates complete, non-destructive three-dimensional reconstruction of both the internal and external surfaces of the analysed sample. Microtomography is widely recognized as the preeminent methodology for characterizing the presence of internal voids in composite laminates. Unlike gravimetric or acid digestion techniques, micro-tomography allows for direct visual analysis of the entire sample volume, allowing researchers not only to verify the absolute void percentage with high precision but also to actively evaluate the complex three-dimensional morphology of individual voids. Furthermore, compared to other conventional methods used to calculate void fraction, X-ray microtomography provides results with a remarkably low standard deviation, ensuring a high degree of statistical reliability. The explicit objective of this tomographic investigation was to map the internal structure of the laminate and confirm the hypotheses regarding the specific causes of the significantly reduced failure load, initially formulated during SEM examination of the fracture surfaces. For both thin and thick specimens, the tomographic scan volume was strictly limited to the central measurement region of the tensile bars, encompassing a targeted extension area of 10 x 10 mm (Fig. 10). Detailed analysis of the reconstructed three-dimensional model was achieved by systematically extracting and evaluating a series of internal cross-sections, oriented along specific planes parallel and perpendicular to the longitudinal direction of the fibre laminate. Sequential examination of these internal tomographic sections provided important information on critical process failures that impacted material performance (Figs. 11 and 12). Analysis of virtual planes sectioned parallel to the lamination direction revealed a clear spatial gradient in defect density; it was evident that the total number of dispersed porosities increased significantly in deeper internal sections of the laminate. This empirical observation demonstrates the difficulty associated with the penetration of viscous resin deep into the dense, non-homogeneous core of the non-woven fabric fibre mat.

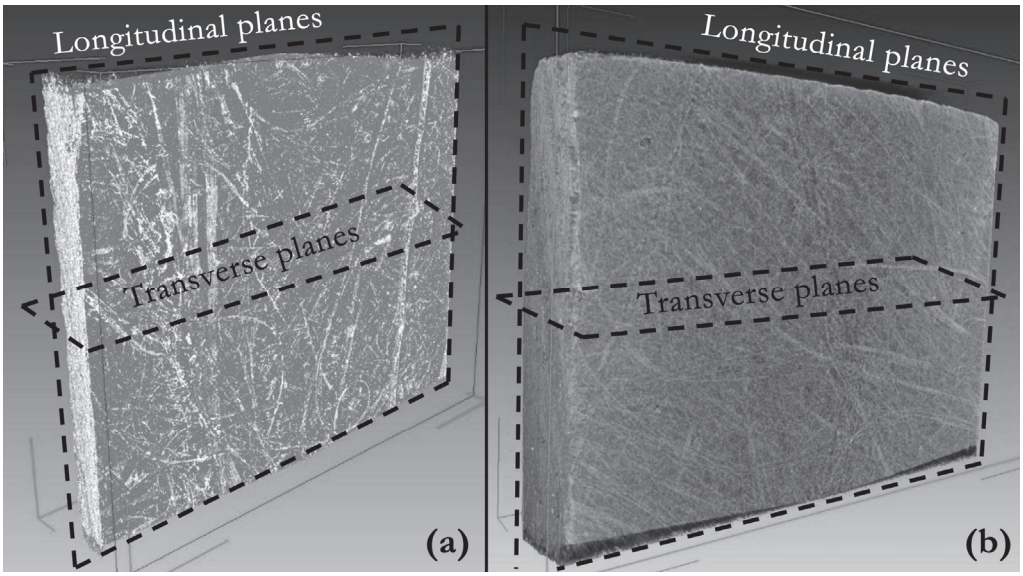

Figure 10: External view of the three-dimensional models of thin (0.8 mm thick) and thick (2.0 mm thick) rCFRP laminate samples, measured by X-ray micro-tomography.

This conclusion was further validated by observing the specific locations where the dense fibre bundles were most concentrated. Tomographic scans confirmed that these densely packed agglomerates directly impeded the uniform propagation of the liquid resin during the critical injection phase. Acting as physical barriers to flow, these bundles forced the advancing resin front to diverge into less resistant preferential paths, an unstable fluid dynamic condition that directly favoured the widespread formation and trapping of massive porosities.

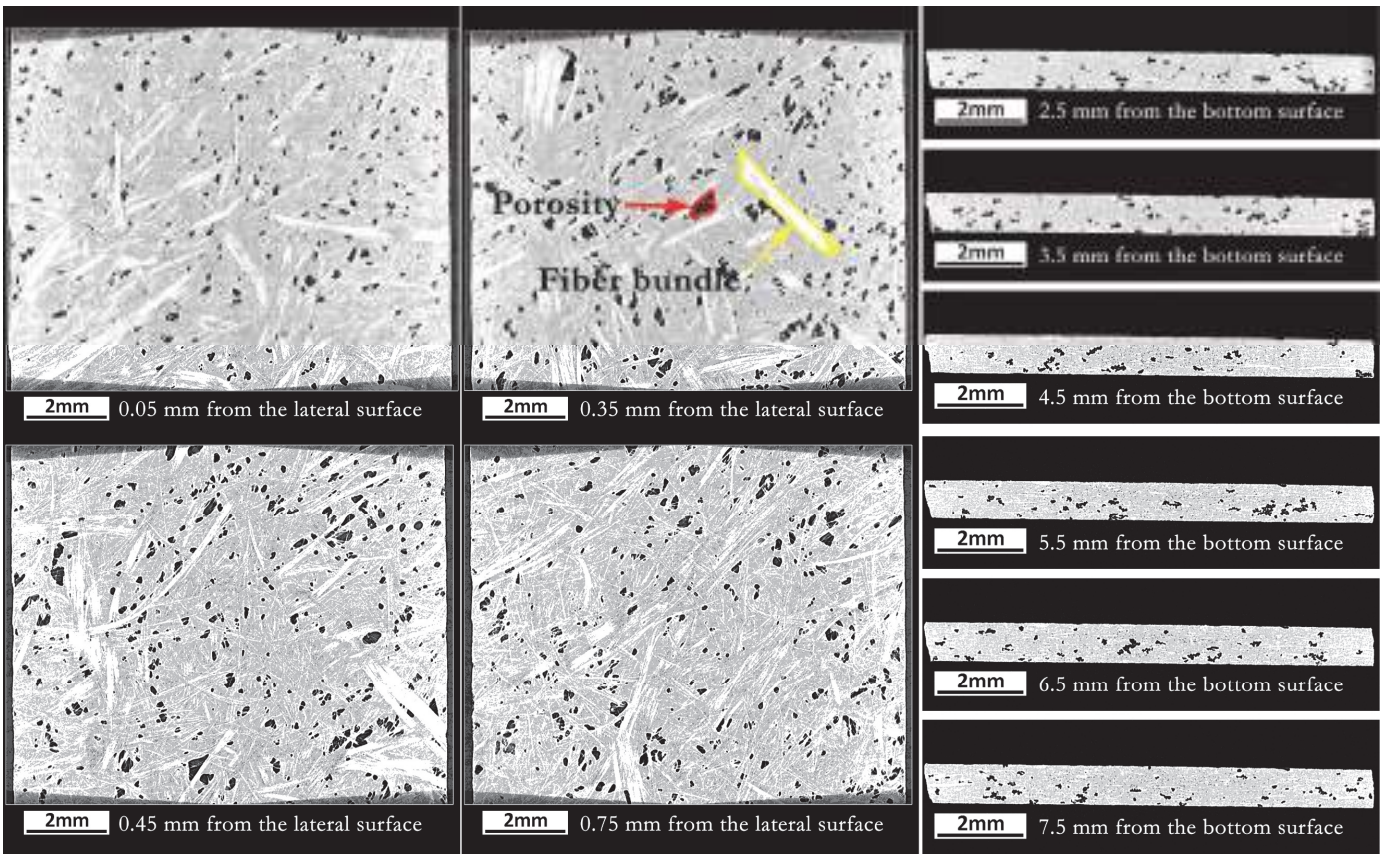

Figure 11: Internal view of the three-dimensional models of the thin specimen (0.8 mm thick) measured by X-ray microtomography. Planes parallel (left) and transverse (right) to the longitudinal direction of the rCFRP laminate.

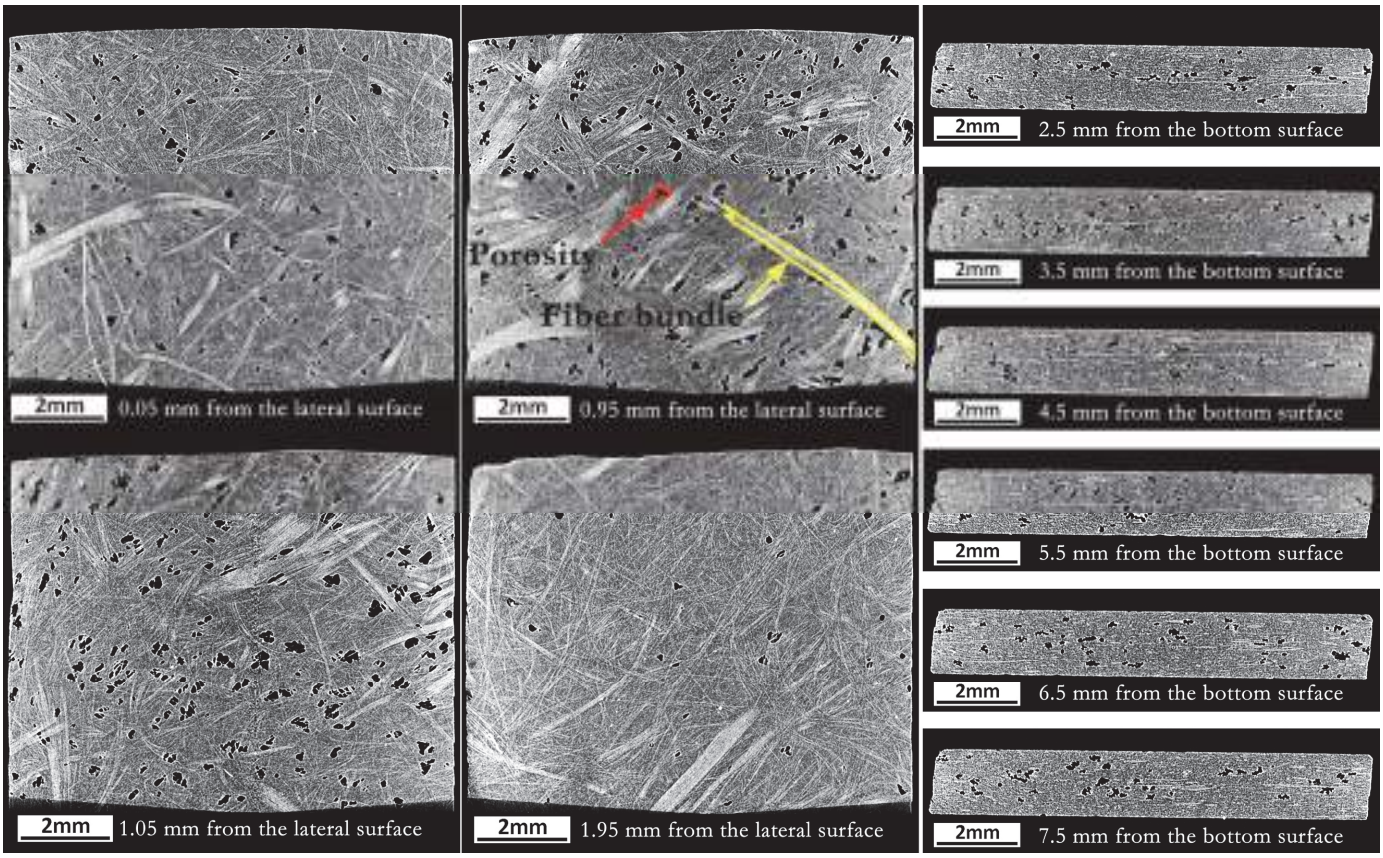

Figure 12: Internal view of the three-dimensional models of the thick specimen (2.0 mm thick) measured by X-ray microtomography. Planes parallel (left) and transverse (right) to the longitudinal direction of the rCFRP laminate.

The tomographic analyses also made it possible to quantitatively evaluate the volume and sphericity of the porosities identified within both laminates (Figs. 13 and 14). From this point of view, sphericity measures how close the porosities are to a perfect sphere, defined as the ratio between the surface area of an equivalent sphere in volume and the effective surface area of the porosity. Sphericity value ranges between 0, meaning a planar defect such as a crack, and 1, representing the perfect spherical void, and constitutes a key parameter for assessing the porosity shape.

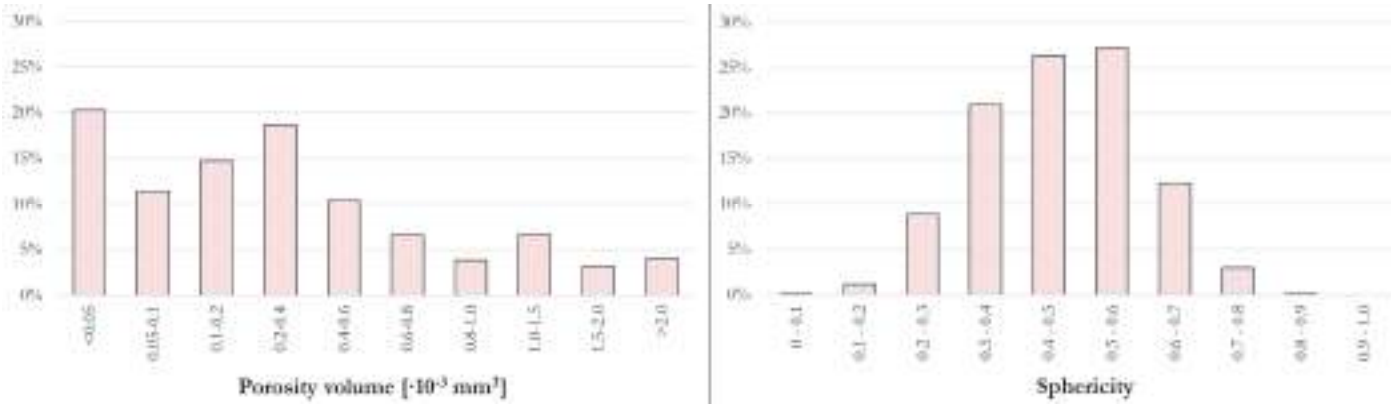

Figure 13: Volume distributions (left) and sphericity (right) of porosities within the thin sample (0.8 mm thickness) measured by X-ray microtomography.

Both laminates show a very similar distribution of both volume and sphericity, highlighting how the shape and size of the porosity are not significantly influenced by the thickness of the laminate (0.8 mm or 2.0 mm). Tomographic data show that porosities varied greatly in scale, ranging from $0.01 \cdot 10^{-3}$ mm³ to $23 \cdot 10^{-3}$ mm³ in volume. For both laminates, approximately two thirds of the porosity has a medium-small volume, less than $0.4 \cdot 10^{-3}$ mm³, while the remaining third exceeds

$0.4 \cdot 10^{-3}$ mm³ until it reaches significant volume, greater than $2 \cdot 10^{-3}$ mm³. For both laminates the sphericity distribution is very close to the Gaussian distribution with a mean of 0.46-0.47 and a standard deviation of 0.12-0.13. In fact, for both plates, over 50% of the porosity has a sphericity between 0.4 and 0.6. These values demonstrate how the shape of the porosity is elongated in the lamination direction and is also conditioned by the irregular arrangement of the carbon fibres.

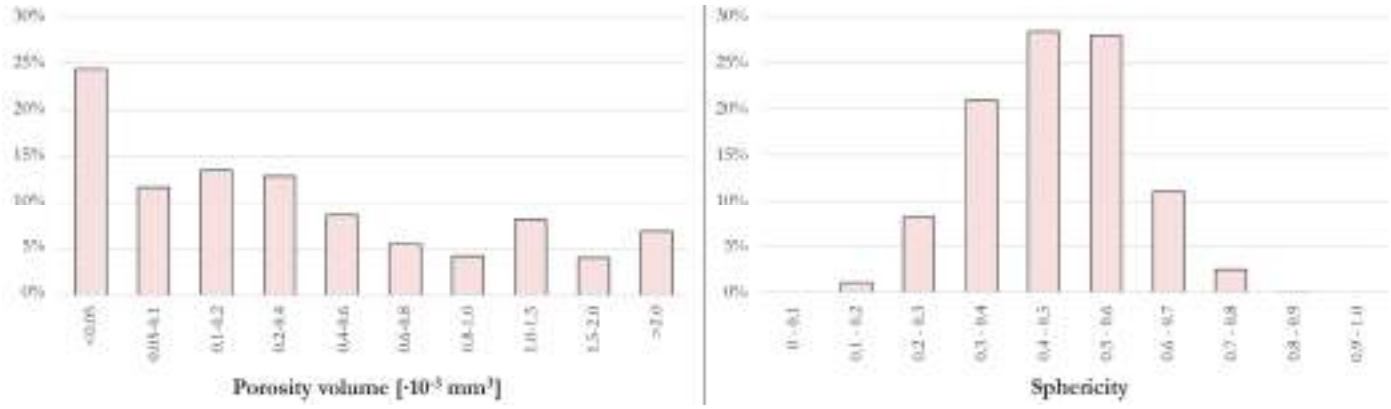

Figure 14: Volume distributions (left) and sphericity (right) of porosities within the thick sample (2.0 mm thickness) measured by X-ray microtomography.

The morphological and dimensional analysis of the internal cavities has suggested two different physical origins for the void formation:

1. *Shrinkage Cavities:* these specific defects are characterized by a highly irregular and jagged shape. Shrinkage voids form almost exclusively during the curing phase, during which the liquid epoxy resin undergoes chemical cross-linking, solidifies, and subsequently physically contracts. On average, during a standard curing cycle, the volumetric shrinkage of a typical aerospace-grade epoxy resin is between 1% and 5% [14]. Because the regions immediately adjacent to the dense fibre bundles already suffer from insufficient localized resin, the internal contraction stresses generated during the shrinkage phase literally tear apart the remaining resin, creating deep, irregular voids.
2. *Air Bubbles:* unlike jagged shrinkage cavities, these specific porosities are defined by their round shape. Air bubbles form primarily during the dynamic phase of resin impregnation. As the resin front advances unevenly across the fibre mat, the air pockets are trapped by the moving polymer.

Tomographic scans also confirmed that the same dense fibre bundles previously identified by surface scanning electron microscopy (SEM) exist as continuous volumetric entities with physical dimensions ranging from 50 μm to 900 μm. Their frequency of occurrence increases dramatically in the deeper and more internal sections of the laminate structure, perfectly supporting the hypothesis of strong spatial inhomogeneity within the initial distribution of recycled fibres non-woven fabric mats. The synthesis of mechanical and tomographic data provides a definitive explanation for the below-expected critical performance of recycled composite panels.

In the field of high-performance composite engineering, typical structurally sound epoxy/carbon laminates exhibit a controlled volumetric void ratio, around 1% - 2%. It is a widely accepted that internal void ratios strictly below 1% can be considered mechanically negligible, having no appreciable negative effect on the final structural properties of the laminate. However, even without performing particularly complex numerical or finite element analysis, tomographic analysis highlights a clear difference between the optimal standard and the real samples. The total void fraction present in the tested laminates is much higher than acceptable thresholds in the aerospace, aeronautical and automotive industries.

It is important to underline that the presence of these voids is catastrophic not only because of the missing volume, but also because their highly irregular shape acts as a strong stress concentrator. These highly localized stress fields easily exceed the UTS of the unreinforced polymer, causing the nucleation and propagation of microcracks that coalesce and reduce the overall tensile strength of the materials, defining brittle behaviour.

CONCLUSIONS

This article aims to provide an in-depth analysis of the mechanical and tomographic properties of recycled CFRP obtained through an innovative, fully mechanical, and environmentally sustainable process [20]. Scanning electron microscopy (SEM) analysis of the extracted recycled fibre non-woven fabric mats revealed excellent cleaning

efficiency; the recovered filaments were almost completely free of polymer matrix residues. Importantly, the recycled fibres showed no signs of degradation, maintaining a constant diameter between 7.0 and 7.5 μm.

Despite the good condition of the recovered fibres, mechanical characterization of the composite laminates (epoxy resin-impregnated panels with thicknesses of 0.8 mm and 2.0 mm) revealed significant performance deficiencies. Tensile tests conducted according to the D3039M standard revealed a high level of anisotropy. Tensile strength (UTS) and Young's modulus (E) recorded the highest values along the longitudinal direction. The thickest laminate (2.0 mm) achieved a maximum longitudinal stress of 310–330 MPa and an elastic modulus of 21.3–21.7 GPa. However, these values are significantly lower than the benchmarks reported in the literature for recycled carbon-epoxy panels with a fibre volume fraction of 27–28%, which typically exhibit an ultimate tensile strength (UTS) of 400–450 MPa and a Young's modulus (E) of 30.0 GPa.

To understand the mechanisms underlying these low failure loads, a rigorous fractographic evaluation was conducted. Visual inspection classified the failure modes predominantly as *"angular"* or *"lateral"* fractures. High-magnification scanning electron microscopy (SEM) analysis of the fracture surfaces revealed the critical flaw: a highly non-uniform spatial distribution of reinforcing fibres within the recycled fibre mat. This nonuniformity manifested itself as dense, agglomerated fibre bundles alternating with large, unreinforced, resin-rich areas. During moulding, the extreme spatial density within these bundles physically impeded microscopic capillary infiltration of the epoxy resin, forcing mass flow to bypass these regions. Consequently, the dry, unimpregnated fibre agglomerates acted as dead zones, while the surrounding resin-rich areas exhibited extreme brittleness, leading to premature and catastrophic fractures.

These hypotheses were confirmed by three-dimensional micro-tomography analysis, which provided a complete volumetric map of the internal defect structure of the laminate. The tomographic cross-sections confirmed a high degree of porosity with a sharp spatial gradient, demonstrating that the porosity concentration increased dramatically in the central sections, confirming the difficulty of resin penetration deep into the dense core of the non-homogeneous fibre mat. The morphological characterization of these internal cavities, with diameters ranging from 50 μm to 700 μm, identified two distinct defect nucleation mechanisms: jagged *"shrinkage cavities"*, due to resin shrinkage in under-impregnated areas, and spherical *"air bubbles"* dynamically trapped by the chaotic resin front during injection.

In conclusion, although the new fully mechanical recycling process is capable of producing mechanically viable carbon fibre non-woven fabric mats, the transformation of these fibres into high-performance structural laminates is currently hampered by serious manufacturing anomalies related to the impregnation process. To close the performance gap, several critical process optimizations are required. First, precise control of resin viscosity and injection pressure is essential to achieve uniform fibre impregnation. To prevent air entrapment, it is strongly recommended to apply a high vacuum inside the mould cavity before resin injection. First, the architectural topology of the starting recycled non-woven fabric mat must be thoroughly revaluated to establish a significantly higher degree of spatial homogeneity, thus preventing the formation of dense aggregates. Implementing these manufacturing guidelines will dramatically reduce internal defects, allowing recycled carbon panels to fully leverage the intrinsic structural value recovered from the cleaning process.

REFERENCES

[1] Gerosa, R., Panzeri, D., Rivolta, B., Casaroli, A. (2023). Deep cryogenic treatment of AA7050: tensile response and corrosion susceptibility, Discover Materials, 3(1). DOI: https://doi.org/10.1007/s43939-023-00037-7.

[2] Gerosa, R., Rivolta, B., Boniardi, M., Casaroli, A. (2022). On the peak strength of 7050 aluminum alloy: mechanical and corrosion resistance, Frattura Ed Integrita Strutturale, 16(60), pp. 273–282. DOI: https://doi.org/10.3221/IGF-ESIS60.19.

[3] Rivolta, B., Boniardi, M.V., Gerosa, R., Casaroli, A., Panzeri, D., Pizetta Zordão, L.H. (2023). Alloy 625 Forgings: Thermo-Metallurgical Model of Solution-Annealing Treatment, J. Mater. Eng. Perform., 32(13), pp. 5785–5797. DOI: https://doi.org/10.1007/s11665-022-07524-7.

[4] Kozaczuk, K.J. (2018). Composite technology development based on helicopter rotor blades, Aircraft Engineering and Aerospace Technology, 92(3), pp. 273–284. DOI: https://doi.org/10.1108/AEAT-12-2017-0260.

[5] Mendi, V., Bathula, V.S., Naidu, D.R., Raminaidu, P., Chinthamreddy, S., Mandula, V. (2025). Strength of rotar blade frequency of helicopter using ANSYS dynamic and harmonic analysis for noise reduction, AIP Conf. Proc., 3325(1), p. 020005. DOI: https://doi.org/10.1063/5.0291837.

[6] Casaroli, A., Scabini, E., Boniardi, M. V., Gerosa, R., Rivolta, B. (2026). Optimization of austenitic and ferritic steels for deep drawing. Part 1: metallurgical and mechanical analyses., Fracture and Structural Integrity, 20(75), pp. 104–123. DOI: https://doi.org/10.3221/IGF-ESIS.75.09.

[7] Casaroli, A., Scabini, E., Boniardi, M. V., Andreotti, R., Rivolta, B. (2026). Optimization of austenitic and ferritic steels for deep drawing. Part 2: FEM analyses with damage development, Fracture and Structural Integrity, 20(75), pp. 179–199. DOI: https://doi.org/10.3221/IGF-ESIS.75.13.
[8] He, H., Gao, F. (2015). Effect of Fiber Volume Fraction on the Flexural Properties of Unidirectional Carbon Fiber/Epoxy Composites, International Journal of Polymer Analysis and Characterization, 20(2), pp. 180–189. DOI: https://doi.org/10.1080/1023666X.2015.989076.
[9] Cox, B.N., Flanagan, G. (1997). Handbook of Analytical Methods for Textile Composites.
[10] Bisheh, H., Abdin, Y. (2023). Carbon Fibers: From PAN to Asphaltene Precursors; A State-of-Art Review, C-Journal of Carbon Research. DOI: https://doi.org/10.3390/c9010019.
[11] Voß, R. (n.d.). ETH Library Fundamentals of Carbon Fibre Reinforced Polymer (CFRP) Machining. DOI: https://doi.org/10.3929/ethz-b-000165454.
[12] Memon, A.W., Memon, S.I., Memon, U.S., Ali, N. (2025). Assessment of the impact of different weave geometries on the crimp factor of woven preforms made from high-performance carbon filaments, Mehran University Research Journal of Engineering and Technology, 44(2), pp. 182–187. DOI: https://doi.org/10.22581/muet1982.3383.
[13] Gupta, J., Reynolds, N., Chiciudean, T., Kendall, K. (2020). A comparative study between epoxy and vinyl ester CF-SMC for high volume automotive composite crash structures, Compos. Struct., 244. DOI: https://doi.org/10.1016/j.compstruct.2020.112299.
[14] Edah, G.O., Atiba, J.O., Fayomi, O.S.I. (2025). Advancements in fibre-reinforced polymers: Properties, applications (A mini review), Next Materials. DOI: https://doi.org/10.1016/j.nxmate.2025.100743.
[15] Yang, Y., Boom, R., Irion, B., van Heerden, D.J., Kuiper, P., de Wit, H. (2012). Recycling of composite materials, Chemical Engineering and Processing: Process Intensification, 51, pp. 53–68. DOI: https://doi.org/10.1016/j.cep.2011.09.007.
[16] Butenegro, J.A., Bahrami, M., Abenojar, J., Martínez, M.Á. (2021). Recent progress in carbon fiber reinforced polymers recycling: A review of recycling methods and reuse of carbon fibers, Materials. DOI: https://doi.org/10.3390/ma14216401.
[17] Kumar, S., Krishnan, S. (2020). Recycling of carbon fiber with epoxy composites by chemical recycling for future perspective: a review, Chemical Papers, pp. 3785–3807. DOI: https://doi.org/10.1007/s11696-020-01198-y.
[18] Aldosari, S.M., AlOtaibi, B.M., Alblalaihid, K.S., Aldoihi, S.A., AlOgab, K.A., Alsaleh, S.S., Alshamary, D.O., Alanazi, T.H., Aldrees, S.D., Alshammari, B.A. (2024). Mechanical Recycling of Carbon Fiber-Reinforced Polymer in a Circular Economy, Polymers (Basel). DOI: https://doi.org/10.3390/polym16101363.
[19] Alrehaili, E., Nurdiawati, A., Al-Ghamdi, S.G. (2025). Sustainable composites for metal replacement: Environmental assessment and material selection of fiber-reinforced polymer across industries, Resources, Conservation and Recycling Advances, 28. DOI: https://doi.org/10.1016/j.rcradv.2025.200294.
[20] Ferrari, P. (2018). Processo di trasformazione di fibre sintetiche e fibre vegetali in tessuto non-tessuto CH 713596A2.
[21] Abdi, B., Wang, Y., Gong, H., Su, M. (2025). Recycling, Remanufacturing and Applications of Semi-Long and Long Carbon Fibre from Waste Composites: A Review, Applied Composite Materials, pp. 1237–1265. DOI: https://doi.org/10.1007/s10443-025-10316-6.
[22] Wang, J., Fuentes, C.A., Zhang, D., Wang, X., Van Vuure, A.W., Seveno, D. (2017). Wettability of carbon fibres at micro- and mesoscales, Carbon N. Y., 120, pp. 438–446. DOI: https://doi.org/10.1016/j.carbon.2017.05.055.